# Feedback of Different Room Geometries on the Sound Generation and Sound Radiation of an Organ Pipe

**Jost Leonhardt Fischer**

*The trick is the idealizations.*
Richard Feynman, Lectures on Physics, Volume I, Chap. 12.1

**Abstract** Feedback effects of different room geometries on the sound generation and sound radiation of an organ pipe is discussed. Motivation of the present work is that in real organs many of the organ pipes cannot radiate sound without disturbance. Most of the organ pipes are mounted, concealed from the audience's view, behind the organ's prospect. Organ pipes of the same stop and with nearly identical timbre are arranged closely on the wind-chest. With several pipe ranks, sound radiated is reflected from pipes as well as from structural elements such as beams or mounting brackets, which hinder free sound radiation. The investigations were carried out by numerical simulations of an organ pipe and its aeroacoustical interaction with several principally different wall geometries as well as swell chambers. The investigation focuses on the effects of reflected sound waves upon the sound generator region of the organ pipe. Several general set-ups were implemented in a numerical space, a pseudo-3*D* computational grid. The numerical simulations were calculated by solving the fully compressible Navier-Stokes equations with suitable initial and boundary conditions for different geometric constraints using a proper LES-model.

## 1 Introduction

In this chapter, the feedback effect of different room geometries on the sound generation and sound radiation of an organ pipe is discussed. The motivation for the present work is the fact that in real organs most of the organ pipes are mounted, concealed from the audience's view, behind the organ's prospect [1]. Pipes of the same organ stop are arranged closely on the wind-chest [1] so that the sound from each pipe cannot radiate without disturbance. Reflections on beams, mounting

J.L. Fischer (✉)
University of Hamburg, Hamburg, Germany
e-mail: jost.leonhardt.fischer@uni-hamburg.de



A. Schneider (ed.), *Studies in Musical Acoustics and Psychoacoustics*,
Current Research in Systematic Musicology 4,
DOI 10.1007/978-3-319-47292-8_4

brackets and other structural elements hinder the free radiation of sound and may influence the sound generation and radiation significantly.

The investigations were carried out by numerical simulations of an organ pipe and its aeroacoustical interaction with several principally different wall geometries. The investigations are focused on the effects of reflected sound waves upon the sound generator region of the organ pipe. The original organ pipe used as template for the numerical model was made by the German organ builder Alexander Schuke Orgelbau Potsdam GmbH [2], cf. Fig. 1a, b.

Several general set-ups were implemented in a numerical space, a pseudo-3*D* computational grid. The numerical simulations were calculated by solving the fully compressible Navier-Stokes equations with suitable initial and boundary conditions for different geometric constraints using a proper LES-model.

The numerical simulations were realized by using parts of the C++ toolbox OpenFoam-2.1. [3]. These libraries include customized numerical solvers as well as pre- and post-processing utilities for the solution of continuum mechanics problems, including computational fluid dynamics (CFD) and computational aeroacoustics (CAA). The code is released as free and open source software under the GNU General Public License. OpenFOAM stands for Open source Field Operation And Manipulation. For details regarding implementation, run and post-processing techniques the reader is referred to the relevant OpenFOAM User Guide and the OpenFOAM Programmer Guide.

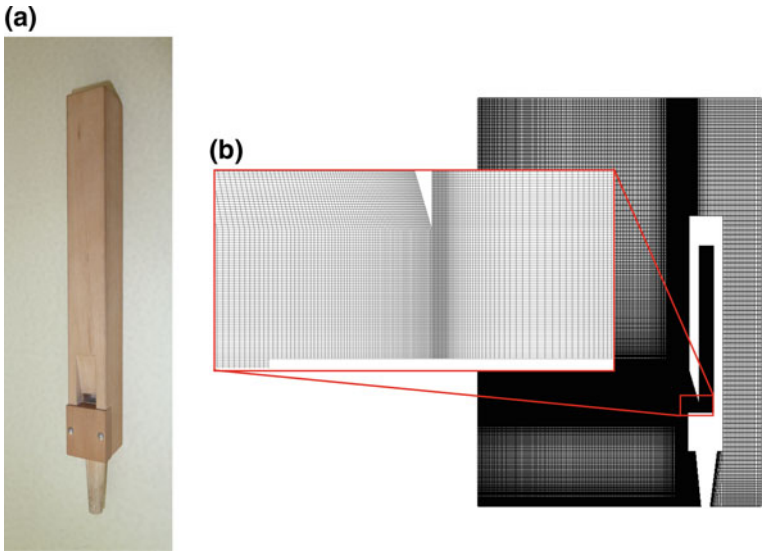


**Fig. 1** **a** Wooden organ pipe with quadratic cross-section, built and provided for measurement use by organ builders Schuke Orgelbau Potsdam GmbH. **b** Implementation of the organ pipe and the surrounding space into a pseudo-3D computational grid. The detail gives an impression of the mesh size in the cut-up region

The first section gives some notes about the general procedure of successful implementation and run of such advanced numerical simulations.

In the second section, the impact of various room geometries on the sound generation of the organ pipe is analyzed at the basis of several particular wall geometries, planar and non-planar geometries. The analyzed wall geometries are representative of conditions that frequently occur in real pipe organ buildings.

The third section addresses the influence of a planar, nearly-closed box geometry, emulating the acoustical conditions of an organ pipe mounted within an open-backed swell chamber. Swell chambers are an integral component of many pipe organs. The organ pipes are mounted within a wooden box equipped with movable shutters towards one, or several, sides which may be mechanically regulated (opened or closed). The swell chamber allows for adding increased dynamic expressiveness to the stop's otherwise rigid behavior, once the instrument maker has finished the intonation process. Examined herein is the influence of the swell chamber geometry on both timbre and frequency spectrum of the organ pipe.

## 2 General Notes on Numerical Implementation and Numerical Simulation

The sound generation in organ pipes, the interaction between flow field (wind field) and acoustical field as well as the sound propagation are described by the compressible Navier-Stokes equations [4, 5]. Hence the compressible Navier-Stokes equations have to be solved with given initial and boundary conditions on a corresponding computational grid, the numerical space, called mesh.

The numerical treatment of compressible problems is an advanced task. In general, a successful procedure of realization can be divided into four sections. (O) Physical previews (A) Pre-processing, (B) Processing and (C) Post-processing. The sections include the following sub-tasks and questions being answered:

O 1. What set of equations describes the problem?
O 2. What characteristic fluid dynamical numbers one has to take into account?
O 3. What are the scales of the problem?
O 4. Hardware-decision
O 5. Software-decision

A 1. How to program a proper mesh?
A 2. Which relevant thermo-physical properties have to be configured?
A 3. Implementation of suitable initial and boundary conditions for physical quantities, e.g. pressure $p$, velocity vector $\vec{U}$, temperature $T$, density $\rho$, turbulent kinetic Energy $k$, etc.
A 4. Appropriate discretization schemes for the operators (Del-operator, Laplacian, time derivative, etc.), inclusive proper correctors

A 5. Identification of an appropriate turbulence model to model the energy transport into the sub-grid scales
A 6. Adequate solver for compressible fluid dynamical problems, determination of numerical schemes and their tolerances
A 7. Adequate matrix solvers
A 8. Configuration of numerical parameter, e.g. numerical time step size, simulation time, write precision etc.
A 9. Definition of suitable probe points and (or) suitable sample sets in the mesh for analysis
B 1. Parallelization of the simulation
B 2. Numerical stability parameter, e.g. Courant number
B 3. Control during simulation run time
B 4. Calculation of additional physical quantities from the data

C 1. Visualization
C 2. Analysis.

For more information, the reader is referred to the author's Ph.D. thesis [6]. General aspects about implementation, pre-processing, run and post-processing numerical simulations can be found in the OpenFOAM User Guide as well as the OpenFOAM Programmer Guide [3].

## 3 The Effect of Complex Geometries

To study the organ sound affected by different spatial geometries, the following scenarios are considered:

| | |
|---|---|
| scenario: *wall* | planar wall at distance 140 mm, |
| scenario: *wall_lambda* | planar wall at distance $\frac{\lambda}{4} = 125$ mm, |
| scenario: *convex* | convex wall, |
| scenario: *concave* | concave wall, |
| scenario: *diffuse* | ridged wall, |
| scenario: *free* | no walls. |

The scenarios were transferred into respective pseudo-3D computational grids. Pseudo-3D means that the mesh besides the x- and y-dimension has also a z-dimension of 10 mm but with only one face in depth. The meshes of the specified scenarios are shown in Fig. 2. The walls considered acoustically inert are marked red. The scenario *free*, which was used as reference scenario has no walls at the boundaries of the numerical set-up. This means that the radiated sound can propagate through the boundaries without any restrictions. The key data of the generated meshes are listed in Table 1. The technique how to write a proper mesh file and how to generate a mesh is documented in the OpenFOAM User Guide [3].

Other configurations, e.g. the initial conditions for the physical quantities velocity $\vec{U}$, pressure $p$, temperature $T$, density $\rho$, turbulent, kinetic energy $k$, etc., thermo-physical

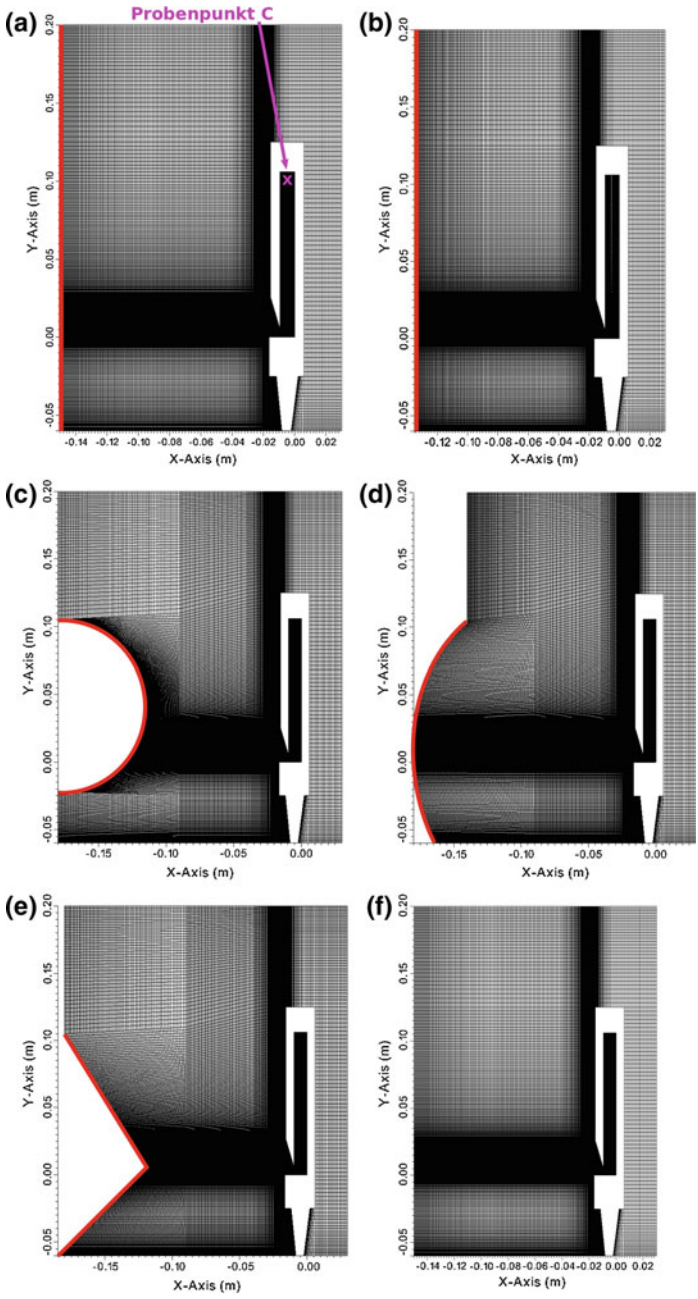


**Fig. 2** The meshes of the scenarios which were investigated. The acoustically inert walls are marked *red*: **a** plane wall (*wall*) at distance 140 mm, **b** plane wall at distance $\lambda/4 = 125$ mm relative to the mouth (*wall_lambda*), **c** convex wall (*convex*), **d** concave wall (*concave*), **e** ridged wall (*diffuse*), **f** free space, without walls (*free*) utilized as reference scenario. The analysis of the scenarios refer to the probe point *C*, which is marked in the mesh of scenario *wall*

**Table 1** Key data of the meshes of the different scenarios

| Scenario | Mesh points | Faces | Hexaeders |
|---|---|---|---|
| *free* | 254342 | 505170 | 126000 |
| *wall* | 254342 | 505170 | 126000 |
| *wall_lambda* | 260362 | 517180 | 129000 |
| *convex* | 260362 | 517180 | 129000 |
| *concave* | 260362 | 517180 | 129000 |
| *diffuse* | 260362 | 517180 | 129000 |

**Table 2** Thermo-physical properties of air at temperature $T = 20$ °C and normal air pressure

| Property | Value | Unit |
|---|---|---|
| Molecules | 1 | |
| Molar mass $M$ | 28.9 | kg/kmol |
| Thermal capacity ($p = const$) $C_p$ | 1007 | J/kg/K |
| Latent heat $h$ | 0 | (off) |
| Dynamic viscosity $\mu$ | $1.8 \times 10^{-5}$ | Ns/m$^2$ |
| Prandtl number $Pr$ | 0.7 | – |

properties, like molar mass $M$ for the medium air, which is assumed as a perfect gas, heat capacity at constant pressure $C_p$, latent heat $h$, dynamic viscosity $\mu$, Prandtl number $Pr$ as well as turbulence properties were implemented. A suitable LES-Model, namely a dynamic SGS-k-model, was choosen. The LES-model includes a transport equation for the turbulent kinetic energy $k$ to calculate the energy transfer into the sub-grid scales (SGS). The thermo-physical properties are summarized in Table 2.

More information about how to implement the mentioned properties can be found in the OpenFOAM User Guide [3]. Visualizations of the numerical simulations are done by the open-source, multi-platform data analysis and visualization application ParaView. Exemplary shown are sequences of the scenario *free* for the quantities pressure $p$ (Fig. 3) and turbulent kinetic energy $k$, (Fig. 4) as well as a sequence of scenario *wall* of the quantity velocity magnitude $|U|$, (Fig. 5).

The analysis mainly refers to the investigation of the pressure at the sample point $C$. The probe point $C$ in all scenarios is 10 mm, centrally located beneath the closed resonator end (cf. Fig. 2). At first, the initial excitation process, called the initial excitation process, is investigated. Then the sound pressure signals of the various scenarios are compared and the sound pressure level spectra (SPL-spectra) are investigated and compared with the corresponding signal of the reference scenario *free*.

## *3.1 The Initial Excitation Process*

During the initial excitation process, the organ pipe ‘finds’ its sound. From a fluid mechanical perspective, in this timespan the initial coupling of the wind field of the inflow and the acoustic field occurs, with the result that in the optimal case a periodic oscillating air sheet is formed, called the jet. The periodical oscillations are

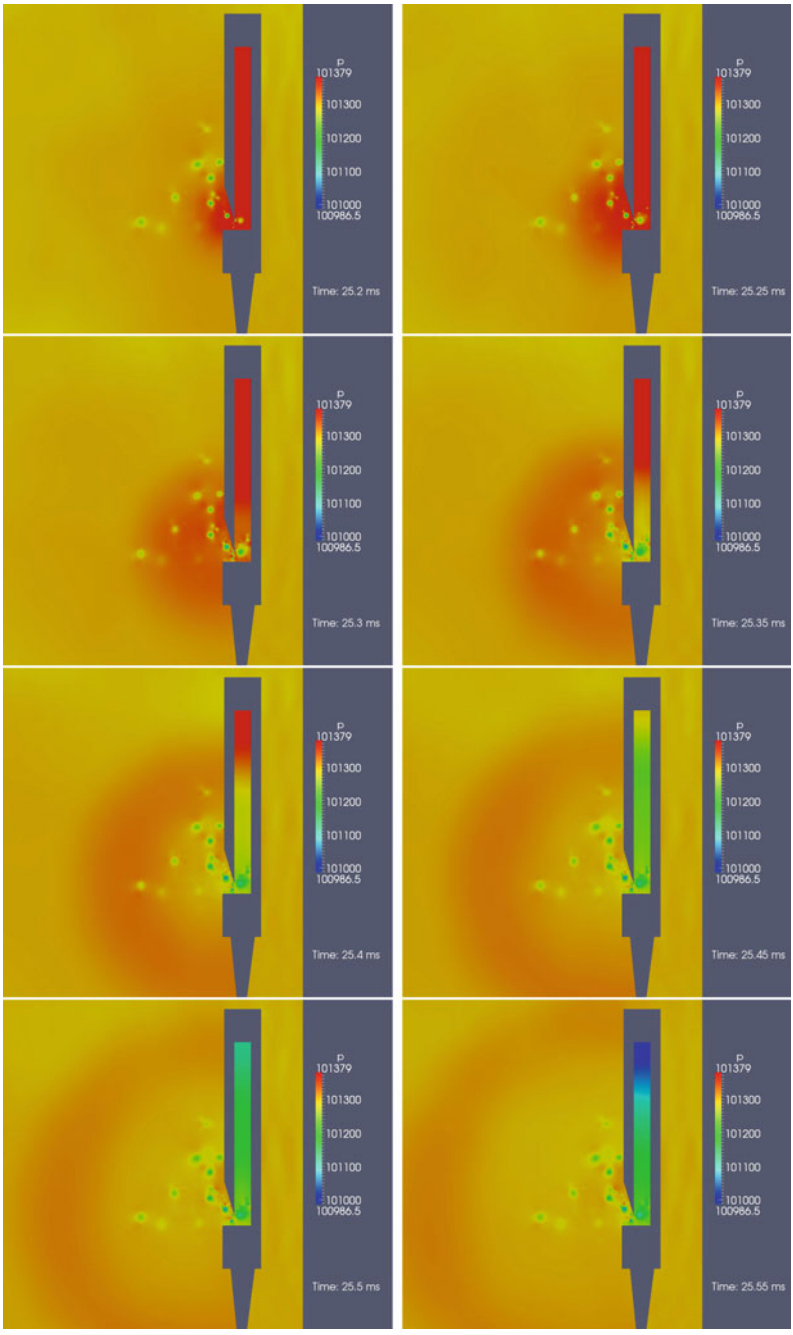


**Fig. 3** Sequence $t = 25.2 - 25.55$ ms of the numerical simulation of scenario *free*. Shown is the pressure $p$. Depicted is the radiation of a sound wave into free space

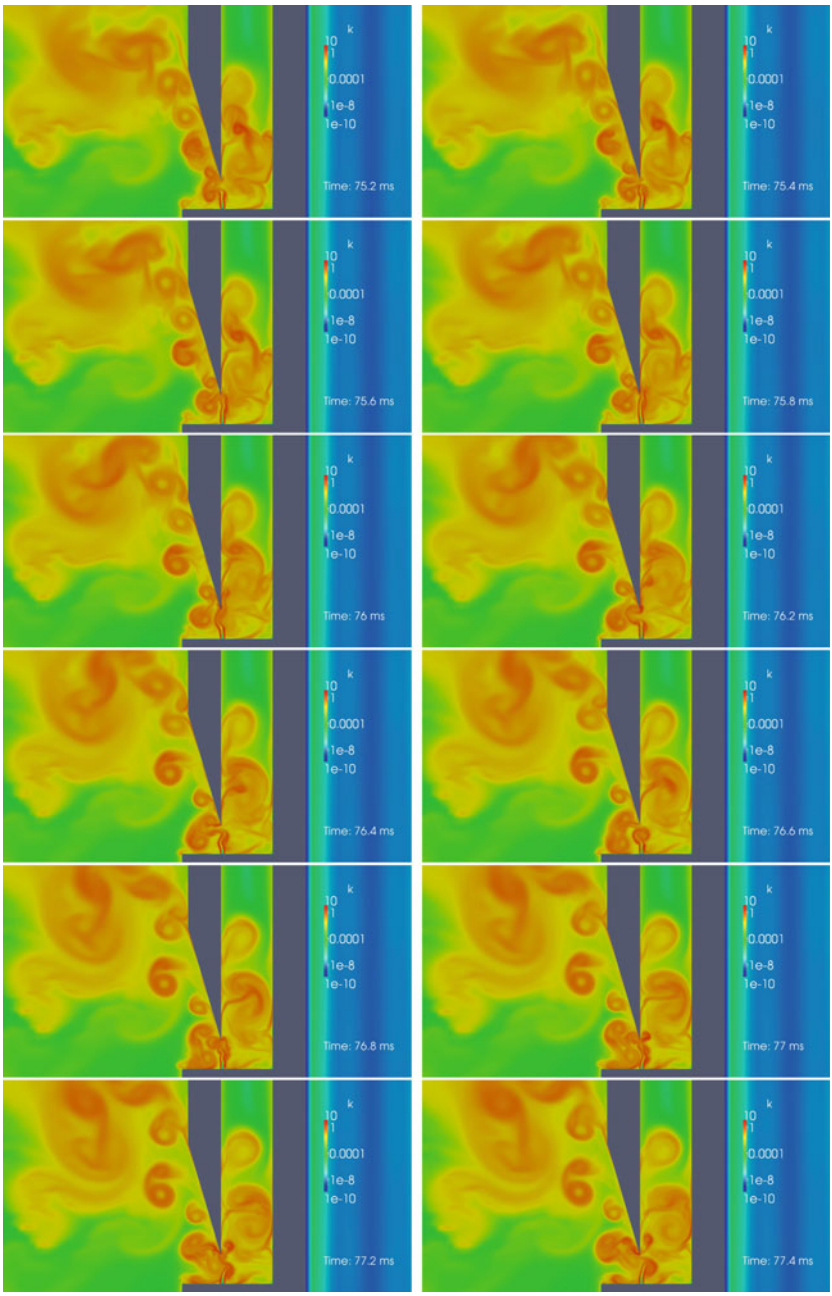


**Fig. 4** Sequence $t = 75.2 - 77.4$ ms of the numerical simulation of scenario *free*. Shown is the log-scaled turbulent kinetic energy $k$. Depicted is the oscillating jet with its shear layers, the formation of vortices inside the resonator as well as a vortex street, escaping the organ pipe along the upper labium

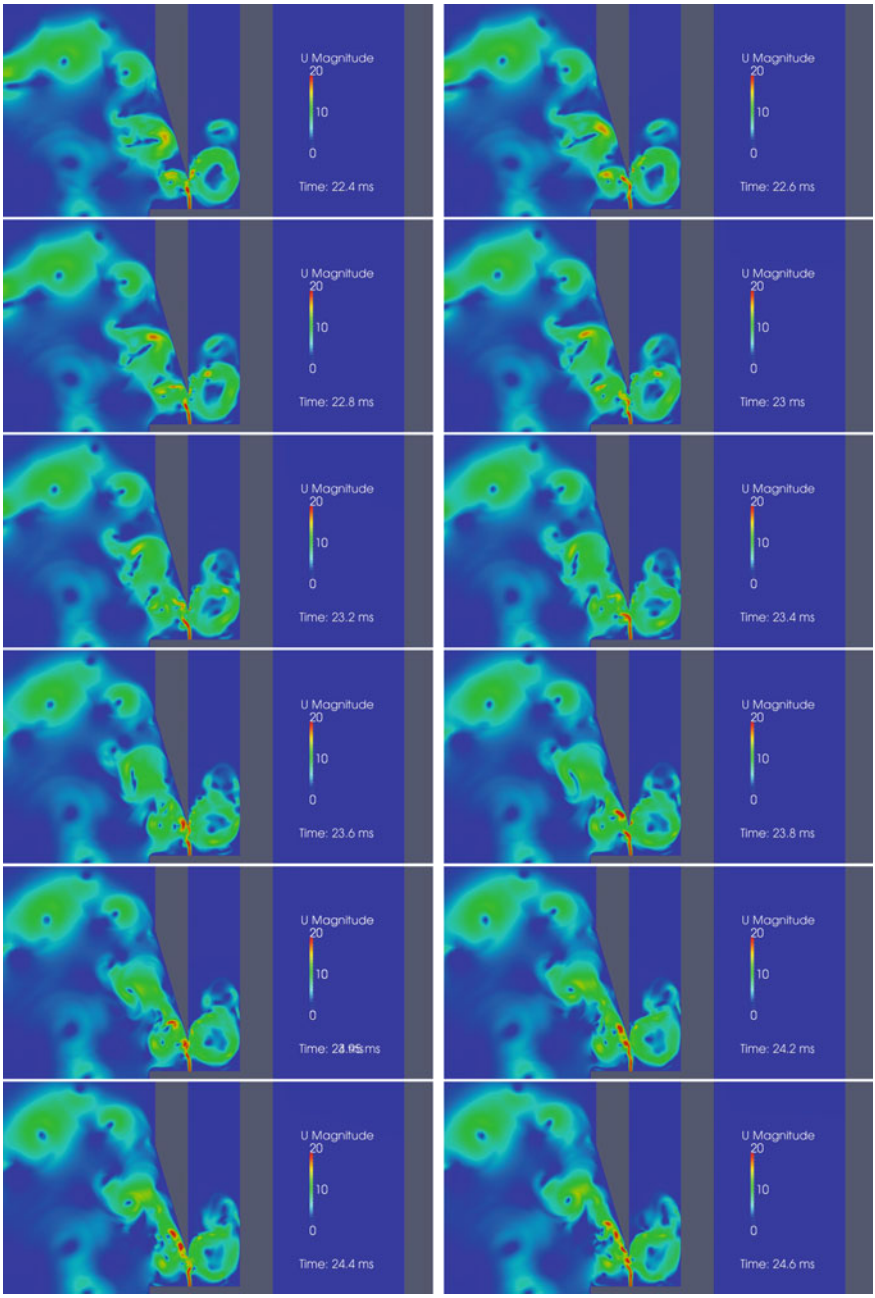


**Fig. 5** Sequence $t = 22.4 - 24.6$ ms of the numerical simulation of scenario *free*. Shown is the velocity magnitude $|U|$. Depicted is the oscillating jet with its shear layers, the formation of vortices inside the resonator as well as a vortex street, escaping the organ pipe along the upper labium

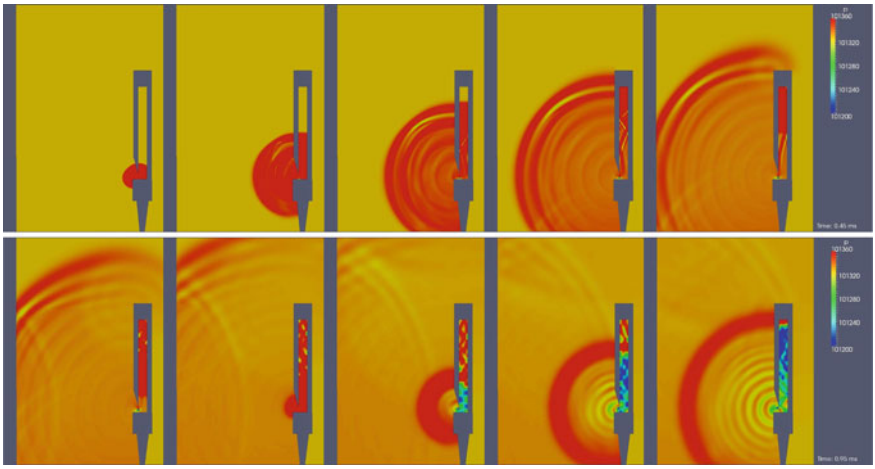

**Fig. 6** Visualization of the radiation of the initial sound waves of a stopped organ pipe in the reference scenario *free*

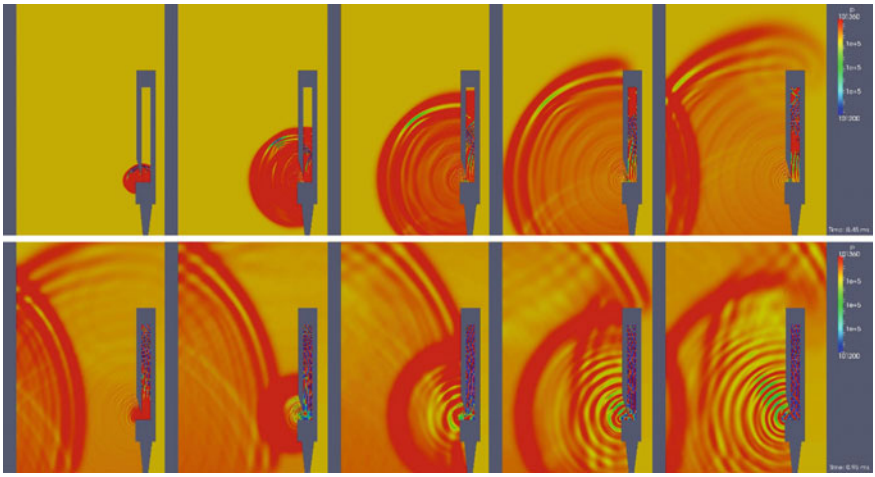

**Fig. 7** Visualization of the radiation of the initial sound waves of a stopped organ pipe in the reference scenario *wall*

transverse to the main direction of the flow. The transient process of initial excitation is dependent on a large number of physical and geometrical parameters such as the wind speed, the size and position of the orifice and the geometry of the mouth. The geometry of the resonator, as well as the geometry of the surrounding room, is this study's object of investigation. The duration of the initial process of excitation lay, in case of the organ pipe examined, in the range of the first 10 ms. Figures 6, 7, 8, 9, 10 and 11 are examples of sequences of the initial excitation for

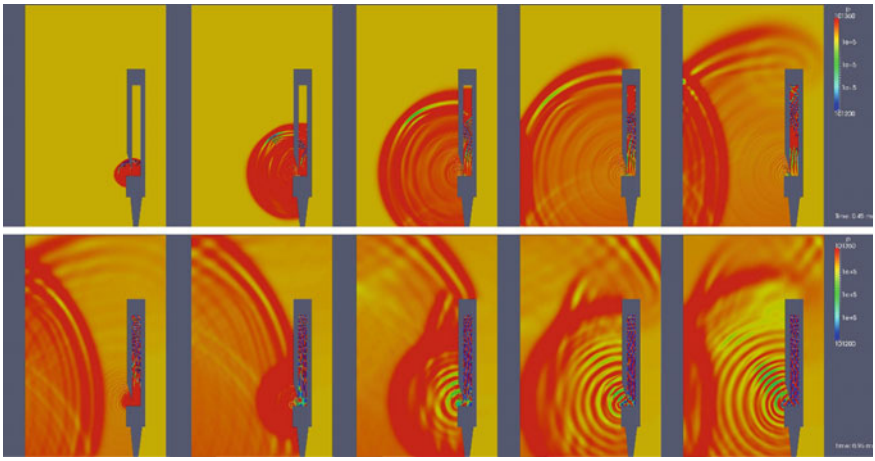

**Fig. 8** Visualization of the radiation of the initial sound waves of a stopped organ pipe in the reference scenario *wall_lambda*

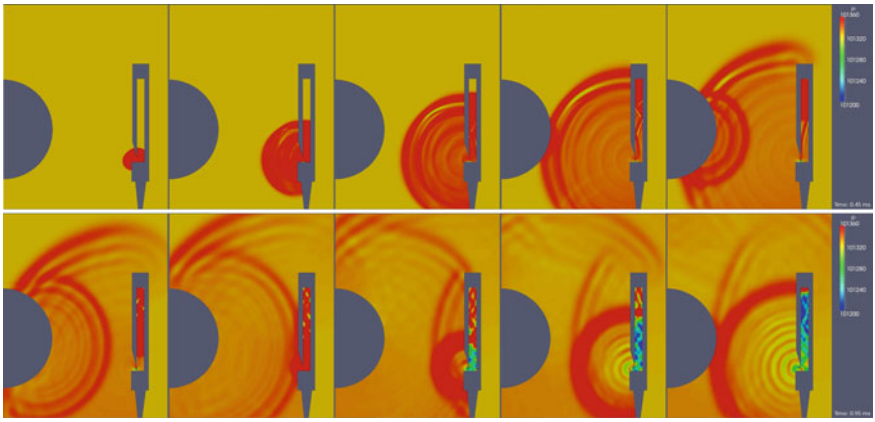

**Fig. 9** Visualization of the radiation of the initial sound waves of a stopped organ pipe in the reference scenario *convex*

scenarios *free*, *wall*, *wall_lambda*, *convex*, *concave* and *diffuse*. It can be seen how the initial sound pressure wave is generated and subsequently radiated into the surrounding room.

The reference scenario *free* shows that sound generation and sound radiation are well represented by the numerical simulation. The propagation of the initial sound pressure wave inside the resonator is clearly shown. Also the transverse modes typical for the initial excitation process are discernable. Because of the pseudo-3D computational grid, the sound pressure wave radiating into the surrounding room appears as a circular shape. For the three-dimensional case, spherical waves are

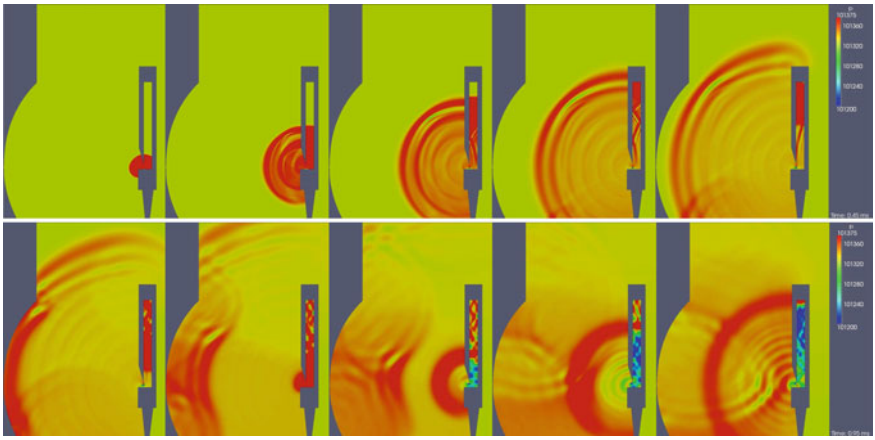

**Fig. 10** Visualization of the radiation of the initial sound waves of a stopped organ pipe in the reference scenario *concave*

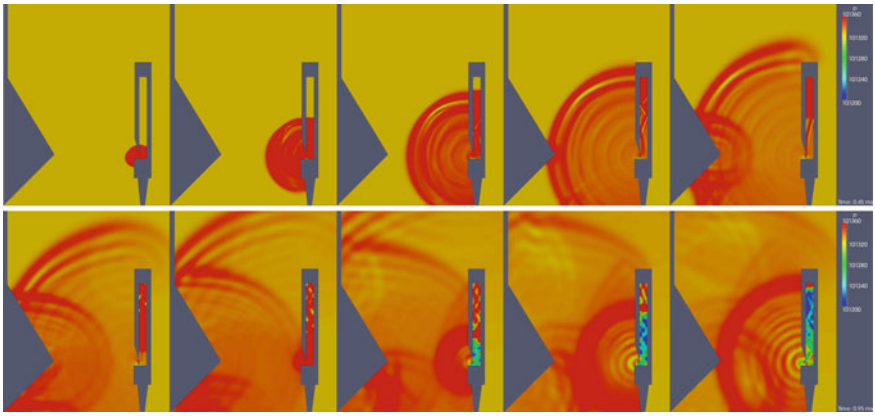

**Fig. 11** Visualization of the radiation of the initial sound waves of a stopped organ pipe in the reference scenario *diffuse*

assumed. Also visible is the radiation of higher harmonics. The scenario's outer margins present a particular challenge, as the boundary conditions have to be defined such that an unimpeded transmission of the propagating physical values is ensured. This means that, within one mesh width, either complete absorption has to be assumed as the boundary condition, this often leading to strong numerical reflections, or a more realistic boundary condition, allowing for the propagation of waves beyond the limits of the computational grid, has to be chosen. Here, the latter variant has been implemented. In the initial conditions for the pressure, respective far field conditions have been specified. At the computational grid's margins, therefore, only comparatively minor numerical reflections occur. They appear at the

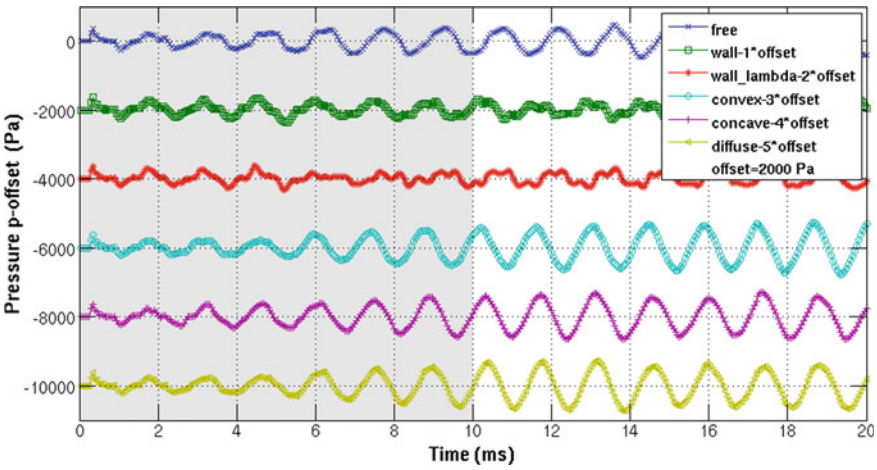


**Fig. 12** The initial excitation process. Shown are the pressure signals of the scenarios sampled at probe point *C*

order of magnitude of the acoustical diffraction phenomena at the upper end of the organ pipe, observable as a bright circle in the first illustration of the second sequence row ($t = 0.55$ ms). Reducing these numerical reflections further by fine tuning the transmission boundary conditions is the aim of current and future research.

Figures 7 and 8 depict sequences of the initial excitation processes of scenarios *wall* and *wall_lambda*. In comparison to the reference scenario *free*, these scenarios show the reflection of the sound wave at the acoustically inert walls. The reflected sound wave propagates back towards the cut-up region of the organ pipe. Observing the radiated higher harmonics in the wake of the initial sound wave, superpositions are clearly visible. Also, the pronounced transverse modes inside the resonator indicate that the reflected sound wave seriously interferes with the periodical movements of the jet. The sound wave is reflected once more at the outer surface of the organ pipe. The space between organ pipe and wall thus becomes a kind of "outer resonator", with the length of the resonator being the distance between wall and cut-up.

The sequence of the initial excitation process of scenario *convex* is shown in Fig. 9. This sequence illustrates how the radiated initial sound wave is reflected at the boundary's convex geometry, propagating back towards the cut-up region as a spherical wave. Note that the radius of the reflected sound wave is smaller than the radii in the scenarios with planar walls. In the sequence of scenario *concave* it can be seen how the initial sound pressure wave is reflected at the boundary's concave geometry, being subsequently focused. In the sequence of scenario *diffuse*, the initial sound pressure wave is reflected at the boundary's ridged geometry, so that the reflected wave is separated.

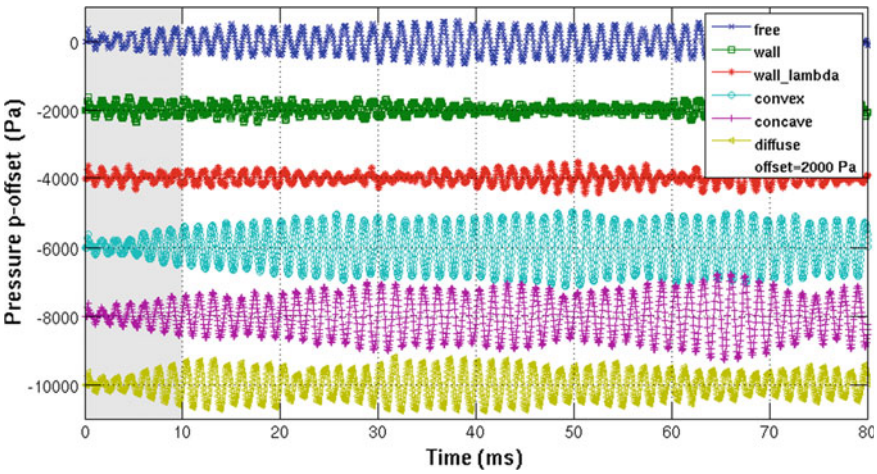


**Fig. 13** The pressure signals sampled at probe point *C* for the different scenarios

In Fig. 12, the sound pressure signals during the initial excitation process are plotted at probe point *C* for all computed scenarios. The initial excitation process is shaded in gray. For reasons of clarity, the signals have been separated by an offset of $-2$ kPa. In the reference scenario *free*, regular, periodic oscillations develop after approximately 10 ms.

In the scenarios *wall* and *wall_lambda* the formation of periodic oscillations is seriously impaired. The disturbances cause a decrease in amplitude as well as a doubling of period. The signals of scenarios *convex*, *concave*, and *diffuse*, on the other hand, exhibit no discernable impairment of the initial excitation process. To the contrary, these scenarios are characterized by a smooth and consistent transient behavior. In comparison to the reference scenario, the developing amplitudes are larger. The oscillations show a triangular waveform, indicating odd-numbered frequencies. Relative to the reference, scenario *diffuse* exhibits a phase shift of $\pi/2$ at $t = 10$ mm. Consequently, the fundamental frequency of the system is higher than in the reference scenario.

The signals resulting from the further course of simulations are shown in Fig. 13. The excitation process again is shaded in gray. The disturbance of the jet in scenarios *wall* and *wall_lambda* leads to a decrease in amplitude as well as to beating. In scenario *wall* the beating exhibits a period of approx. $T_S = 100$ ms, corresponding to beat frequencies of approx. $f_S = 10.0$ Hz and $f_S = 16.5$ Hz, respectively. Beating can only be induced by the superposition of several different frequencies. This implies that a plane wall acts as a significant obstacle to sound radiation, causing attenuation in the amplitude domain as well as amplification in the frequency domain.

The pressure signal in scenario *convex*, at sample point *C*, exhibits the most regular waveform of all scenarios, including the reference scenario *free*. Amplitudes are consistently larger compared to the reference case. Furthermore, a slight

increase in frequency is observed. The results show that this geometry leads to an amplification in both the amplitude and frequency domains.

In scenario *concave*, the largest amplitudes are observed. This is caused by the wall's concave geometry focussing the reflected sound wave. The amplitudes of the signal are, however, less evenly distributed when compared with *convex*, perhaps also due to beating.

The waveform of scenario *diffuse* is also uneven and exhibits beating. Also, the separation and diversion of the reflected sound wave causes lower amplitudes.

## 3.2 Sound Pressure Level Spectra

Based on the pressure signals at probe point $C$, as obtained by numerical simulation, sound pressure level spectra are generated. Here the signals obtained over the simulation's entire duration of $t_{sim} = 100\,\text{ms}$ are utilized. The sampling frequency is the inverse of the sampling interval. In the numerical simulations, this is the temporal increment displayed as $\Delta t_s = 5 \times 10^{-6}\,\text{s}$. This results in a sampling frequency of $f_s = 20000\,\text{Hz}$ .

First, the extracted signals are transformed into amplitude spectra by means of Fourier transformation. The concept of Fourier transformation constitutes the notion that any periodic function with a period $T$ can be expressed as the sum of a, generally infinite, number of harmonic oscillations with their respective specific frequencies being integral multiples of the fundamental frequency $f_0$. In the case of the function being a discrete signal, the decomposition by Fourier is, assuming $\omega_0 = 2\pi/T = 2\pi f_0$, expressed as

$$f(t) = c_0 + \left[\sum_{n=1}^{\infty} a_n \cdot \cos(n\omega_o t) + b_n \cdot \sin(n\omega_0 t)\right] \tag{1}$$

The coefficients $a_n(n\omega_0)$ and $b_n(n\omega_0)$ are called the Fourier coefficients. To determine the Fourier coefficients is the subject matter of Fourier analysis. One finds

$$c_0 = \frac{1}{T}\int_{-\frac{T}{2}}^{\frac{T}{2}} f(t)\,dt \tag{2}$$

$$a_n = \frac{2}{T}\int_{-\frac{T}{2}}^{\frac{T}{2}} f(t) \cdot \cos(n\omega_0 t)\,dt \quad n = 0, 1, 2, 3, \ldots \tag{3}$$

$$b_n = \frac{2}{T} \int_{-\frac{T}{2}}^{\frac{T}{2}} f(t) \cdot \sin(n\omega_0 t)\, dt \quad n = 0, 1, 2, 3, \ldots \tag{4}$$

The Fourier coefficient $c_0$ is the temporal average of the signal $f(t)$ taken over one period, also referred to as steady component, or as the signal's offset (in electrical engineering called DC-component).

Taking the relations

$$a_n \cos(n\omega_0 t) + b_n \sin(n\omega_0 t) = c_n \sin(n\omega_0 t + \phi_n) \tag{5}$$

and

$$c_n = \sqrt{a_n^2 + b_n^2} \tag{6}$$

$$\phi_n = \arctan\left(\frac{a_n}{b_n}\right) \tag{7}$$

one finally obtains the **spectral representation** of the Fourier series

$$f(\omega) = c_0 + \sum_{n=1}^{\infty} c_n \sin(n\omega_0 t + \phi_n) \tag{8}$$

A periodic signal is thus determined by the values for

| | |
|---|---|
| $c_0$ | Temporal average over one period of the signal f(t), |
| $c_n = c_n(n\omega_0)$ | Amplitude spectrum, |
| $\phi_n = \phi_n(n\omega_0)$ | Phase spectrum. |

Taking the amplitude spectrum, the sound pressure level spectrum (SPL-spectrum) is calculated by

$$\mathrm{SPL} = 20 \cdot \log_{10}\left(\frac{p_{rms}}{p_0}\right) \mathrm{dB} \tag{9}$$

with the pressure's root mean square value $p_{rms} = p/\sqrt{2}$ and the reference pressure being $p_0 = 20\,\mu\mathrm{Pa}$.

Figure 14 shows the sound pressure level spectra obtained. In Tables 3 and 4 the frequencies and amplitudes of the fundamentals as well as of the 2nd, 3rd, and 5th harmonics are summarized. The frequency resolution of the numeric simulation's level spectra result from the inverse of the simulation's duration and amounts to $\Delta f = \pm 5\,\mathrm{Hz}$.

All level spectra exhibit a prominent fundamental oscillation. Compared to the spectrum of reference scenario *free*, the largest increase in frequency is to be found

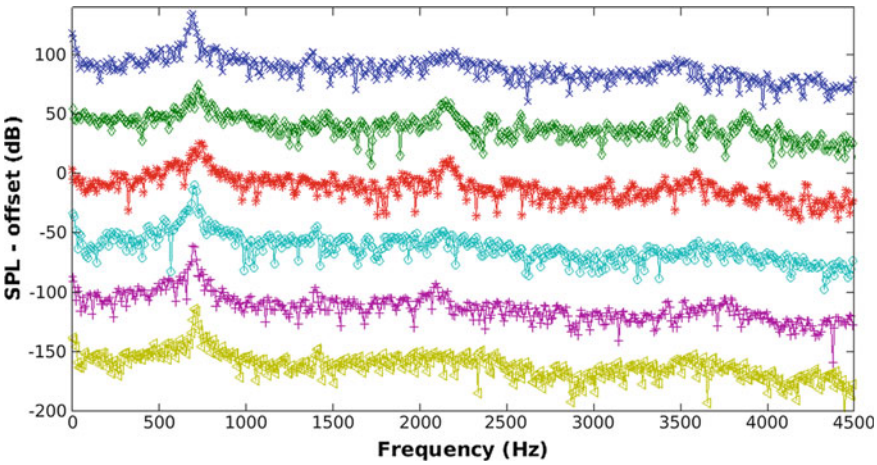


**Fig. 14** SPL-spectra at the probe point *C* for the scenarios, top down, *free*, *wall*, *wall_lambda*, *convex*, *concave* and *diffuse*. Shown are the spectra of sound pressure level in the range of frequency of $0 - 4500$ Hz. For reasons of clarity the spectra are separated by an offset of $-50$ dB. The SPL-scale is related to the reference scenario *free*. One sees prominent fundamentals, 2nd harmonics with low amplitudes, 3rd, and 5th harmonics

**Table 3** Frequencies of the fundamentals, the 2nd, 3rd and 5th harmonics sampled at probe point *C*

| Frequency/scenario | Fundamental (±5 Hz) | 2. Harm. (±5 Hz) | 3. Harm. (±5 Hz) | 5. Harm. (±5 Hz) |
|---|---|---|---|---|
| *free* | 693 | 1377 | 2207 | 3477 |
| *wall* | 723 | 1465 | 2148 | 3496 |
| *wall_lambda* | 742 | 1507 | 2178 | 3594 |
| *convex* | 703 | 1406 | 2129 | 3604 |
| *concave* | 693 | 1396 | 2090 | 3750 |
| *diffuse* | 703 | 1416 | 2002 | 3574 |

**Table 4** SPL-spectra of the fundamentals, the 2nd, 3rd, and 5th harmonics sampled at probe point *C*

| SPL/scenario | Fundamental (dB) | 2. Harm. (dB) | 3. Harm. (dB) | 5. Harm. (dB) |
|---|---|---|---|---|
| *free* | 131.5 | 99.5 | 100.5 | 93.5 |
| *wall* | 121.5 | 97.5 | 106.5 | 102.5 |
| *wall_lambda* | 122.5 | 96.5 | 109.5 | 98.5 |
| *convex* | 137.5 | 101.5 | 97.5 | 89.5 |
| *concave* | 136.5 | 100.5 | 104.5 | 92.5 |
| *diffuse* | 132.5 | 99.5 | 96.5 | 94.5 |

in scenarios *wall* and *wall_lambda*. They amount to $30 \pm 5\,Hz$ and $49 \pm 5$ Hz, respectively. The level of the 3rd and 5th harmonics, furthermore, are significantly emphasized. One finds increases in level of +6 and +9 dB of the respective frequencies, cf. Table 3.

Scenario *convex* is distinguished by the accentuation of the fundamental oscillation when compared to the reference scenario. The level is raised by $+6$ dB as against scenario *free*, meaning a doubling of the fundamental oscillation's loudness. All other harmonics, on the other hand, are slightly attenuated.

In scenario *concave*, there is an increase in level of the fundamental as well as the 3rd harmonic, caused by the concave geometry. The ridged geometry in scenario *diffuse* accentuates the fundamental and attenuates the 3rd harmonic.

In all scenarios, the 2nd harmonic can be observed. The occurrence of the second harmonic in a stopped organ pipe is, admittedly, mathematically impossible according to linear wave theory. Organ builders, however, are familiar with this effect in their practical work. The cause for the occurrence of the 2nd harmonic is the formation of an oscillating acoustic dipole at the tip of the labium [7]. The dipole changes its configuration twice within each of the jet's periods, i.e., it oscillates with twice the jet's frequency. The level of the 2nd harmonics observed in the numerical simulation are usually smaller than the levels of the fundamentals and the 3rd harmonics; this is in agreement with practical experience. The attenuation of higher harmonics as observed in scenarios *convex* and *diffuse* leads, however, to the 2nd harmonic obtaining a certain sonic significance. The occurrence of 2nd harmonics in the numerical simulation attests for its high accuracy and realism.

## 3.3 Phase Portraits

Taking the time derivative of the scenarios' pressure signals, and plotting $dp/dt$ against $p$, the results are the phase portraits of the oscillating pressure at probe point $C$ (cf. [7]). The phase portraits provide information about the similarity of the observed oscillations to known types of oscillators. An harmonic oscillator, for example, displays a closed circular trajectory; a damped harmonic oscillator with positive damping displays a spiral shape wound around a stable central fixpoint; an excited harmonic oscillator, having negative damping, displays a spiral shape winding itself away from an instable central fixpoint. A self-excited oscillator, a resonator with nonlinear damping, displays a limit cycle. Depending on the degree of nonlinearity, its phase portrait exhibits a more or less deformed circle. Figure 15a–d as exemplary models show the phase portraits of different oscillator types.

In Fig. 16a–f, the smoothed phase portraits of the different scenarios within the range t = 10–80 ms of the numerical simulations are shown. Figure 17a–f show the normalized phase portraits. The transient excitation process is truncated. Highly dissimilar trajectories can be seen. With the signals being constantly subjected to external interferences, no cohesive trajectories, as described in theory, are observed. The scenarios indeed represent extensive aeroacoustic, and in a sense 'real',

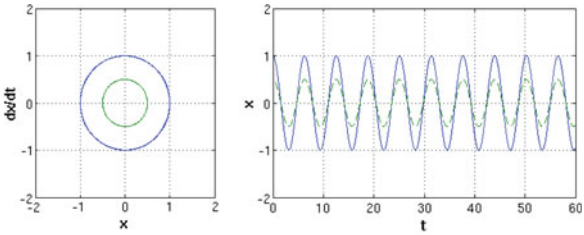


**(a)** The harmonic oscillator: $\ddot{x} + \omega_0^2 x = 0, \omega_0 = 1.0$. Shown are two solutions for the initial conditions: $x_1(0) = 1.0, \dot{x}_1 = 0.0$, and $x_2(0) = 0.5, \dot{x}_2 = 0.0$.

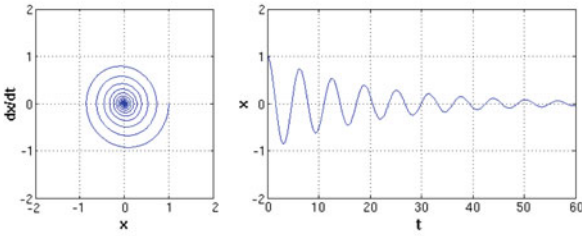


**(b)** A damped harmonic oscillator:
$\ddot{x} + \gamma\dot{x} + \omega_0^2 x = 0, \omega_0 = 1.0, \gamma = 0.1$. The initial conditions are:
$x(0) = 1.0, \dot{x} = 0.0$

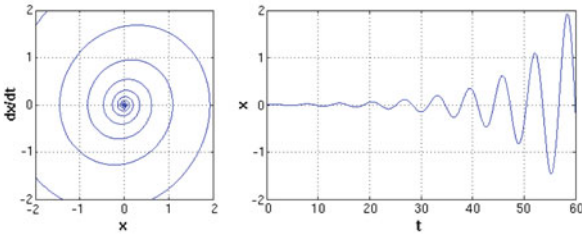


**(c)** A negatively damped harmonic oscillator:
$\ddot{x} + \gamma\dot{x} + \omega_0^2 x = 0$, $\omega_0 = 1.0, \gamma = -0.18$. The initial conditions are:
$x(0) = 0.0, \dot{x} = 0.01$

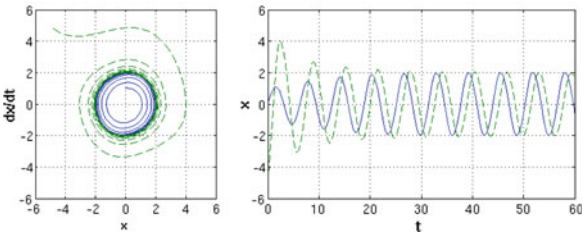


**(d)** A self-sustained oscillator type, the Van der Pol oscillator:
$\ddot{x} - \mu\left(1 - x^2\right)\dot{x} + \omega_0^2 = 0$, $\omega_0 = 1.0, \mu = 0.08$. The initial conditions of the two solutions are:
$x_1(0) = 0.0, \dot{x}_1 = 1.0, x_2(0) = -5.0, \dot{x}_2 = 5.0$

**Fig. 15** **a** The harmonic oscillator as an example of a conservative system. The total energy of the system is constant. **b** The damped harmonic oscillator, a dissipative system. Energy gets lost. **c** The harmonic oscillator with a negative damping term, an (internal) excitative system. Energy is supplied. **d** The Van der Pol oscillator as an example of a self-sustained oscillator. The system balances dissipation and internal excitation. After a transient timespan the system oscillates at the limit cycle

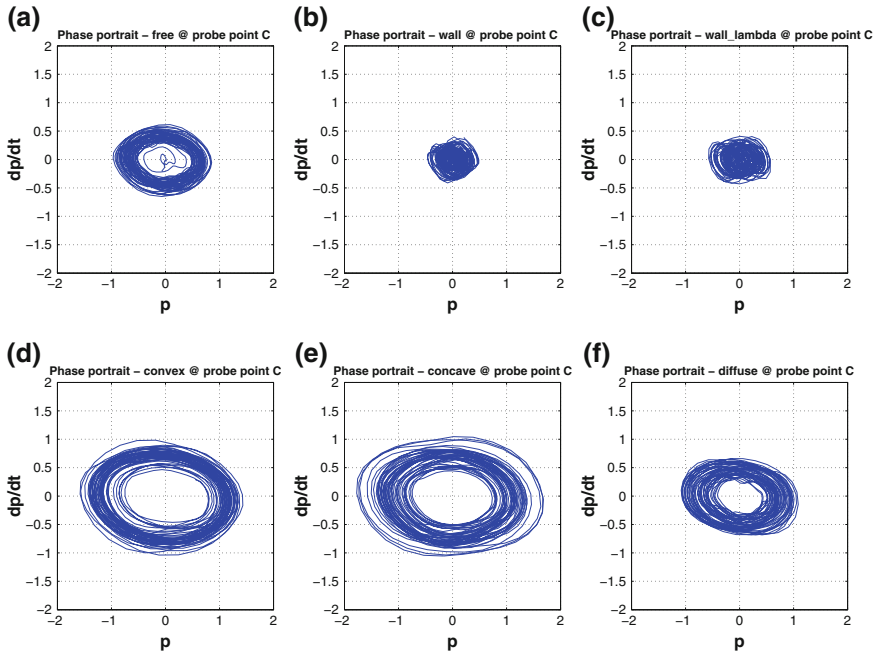


**Fig. 16** Phase portraits of the scenarios **a** *free*, **b** *wall*, **c** *wall_lambda*, **d** *convex*, **e** *concave* and **f** *diffuse*. From the full simulation timespan of $t_{sim} = 100$ ms the part $t = 10-80$ ms is depicted.

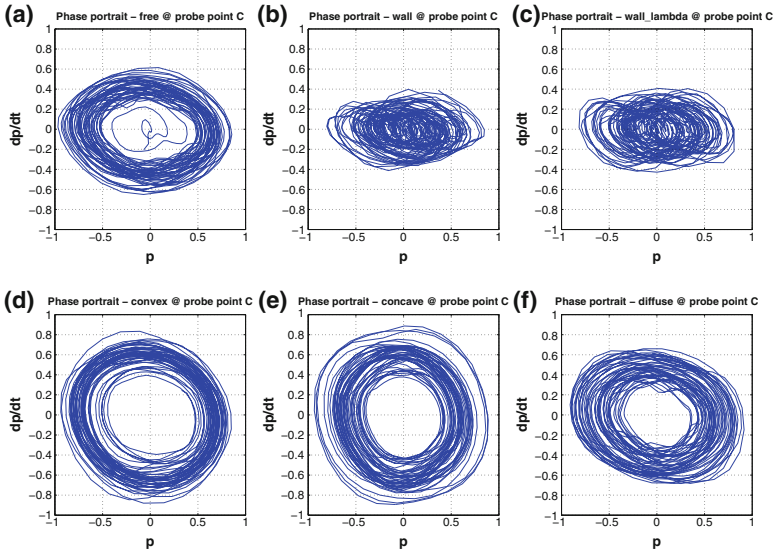


**Fig. 17** Normalized phase portraits of the scenarios **a** *free*, **b** *wall*, **c** *wall_lambda*, **d** *convex*, **e** *concave* and **f** *diffuse*. The timespan depicted is t = 10−80 ms

oscillator systems. Nevertheless, it is recognizable that all scenarios represent self-sustained oscillator systems.

The phase portraits of scenarios *wall* and *wall_lambda* show strong disturbances, which prevent the formation of larger amplitudes. The doubling of period mentioned above can be clearly seen in Figs. 17b, c.

The trajectories in the phase portrait of scenario *convex* are elliptical, and circular in the normalized representation in Fig. 17d, thus resembling that of a harmonic oscillator. The course of the trajectories of scenario *concave* rather reminds one more of a tilted square than of a circle, this being especially the case with the outer trajectories.

Perhaps this is the matter of a second oscillatory regime with larger amplitudes into which the system transitions in case sufficient energy is available. This might be caused by the focusing of the incoming sound waves, an issue that, however, will not be treated within the scope of this article. In any case, a substantial change within the self-excited oscillatory behavior can be observed in comparison to the reference scenario *free*.

The spatial orientation of the trajectories in the phase portrait of scenario *diffuse* deviates considerably from those of the other scenarios. The phase portrait appears to be tilted clockwise. The pressure's zero crossings do not coincide with the points of maximum pressure change, implying a phase shift between these values in the order of $\Delta\phi \approx \pi/8$.

The phase portraits attest to the considerable influence of different spatial geometries on the sound generation process within the organ pipe. The nonlinearities within the system are significantly affected by the surrounding spatial geometry. This can be observed as deformations of the trajectories' regimes, as shown in the phase portraits. The non-linear oscillations within the organ pipe are being downright 'reshaped' through the influence of the different geometry. Depending on the type of spatial geometry, certain frequencies are either being accentuated or attenuated, leading to a significant change in the organ pipe's timbre.

## 4 The Feedback Effect of Swell Chamber Geometries

In this section, the feedback effect of the swell chamber geometry on the sound generation and sound radiation of an organ pipe is addressed. This part of the study evaluates the results of two numerical simulations, taking into account different swell chamber boundary conditions. In the first part, the geometries applied are briefly discussed. Following this, the computational execution of the simulation is outlined. In the third part, the results of the simulation are analyzed and compared to the results of the reference scenario *free*. This survey concludes with a brief summary as well as an outlook towards future work.

The numerical simulation is performed on the basis of a wooden stopped organ pipe having a quadratic cross-section and a fundamental frequency of $f = 700\,\mathrm{Hz}$,

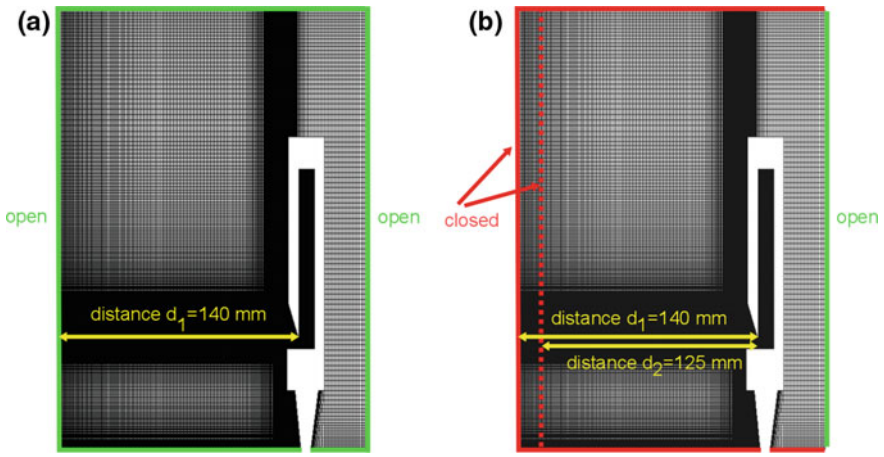


**Fig. 18** Schematic description of the boundary conditions of the numerical simulations, **a** reference scenario *free*, **b** the scenarios *swell_140* mm and *swell_125* mm, with a wall distance of 140 mm and 125 mm to the pipes mouth

as shown in Fig. 1a. The organ pipe was custom-built by organ makers Schuke Orgelbau Potsdam GmbH [2] and provided for measurement use. The geometry of the organ pipe as well as the near-field ambient space are translated into a pseudo-3D computational grid by the procedure described in Sect. 3; the computational grid is shown in Fig. 1b.

The key data of the computational grid used are those of scenario *free* (cf. Table 1). The thermo-physical properties are summarized in Table 2.

In terms of boundary conditions for the room, two different configurations are implemented. Their geometries are equivalent to those of scenarios *wall* and *wall_lambda*, in this case, however, exhibiting three acoustically inert surfaces: the floor, the wall opposite the cut-up, and the ceiling. Only the numerical boundary behind the organ pipe remains open. The boundary conditions of the reference scenario *free* and the configurations *swell_140* mm and *swell_125* mm are shown in Fig. 18a, b. No-slip boundary conditions are chosen for the organ pipe's inside and outside walls as well as for the walls of the swell chamber. For the organ pipe's windway, i.e., the inlet and the open room boundaries herein referred to as outlet, boundary conditions are chosen that ensure conservation of mass.

## *4.1 Numerical Simulations of an Organ Pipe within Swell Chambers*

Each run of the simulation generates a data volume of approximately 80 GB. From the total amount of generated data, animated sequences are compiled for the

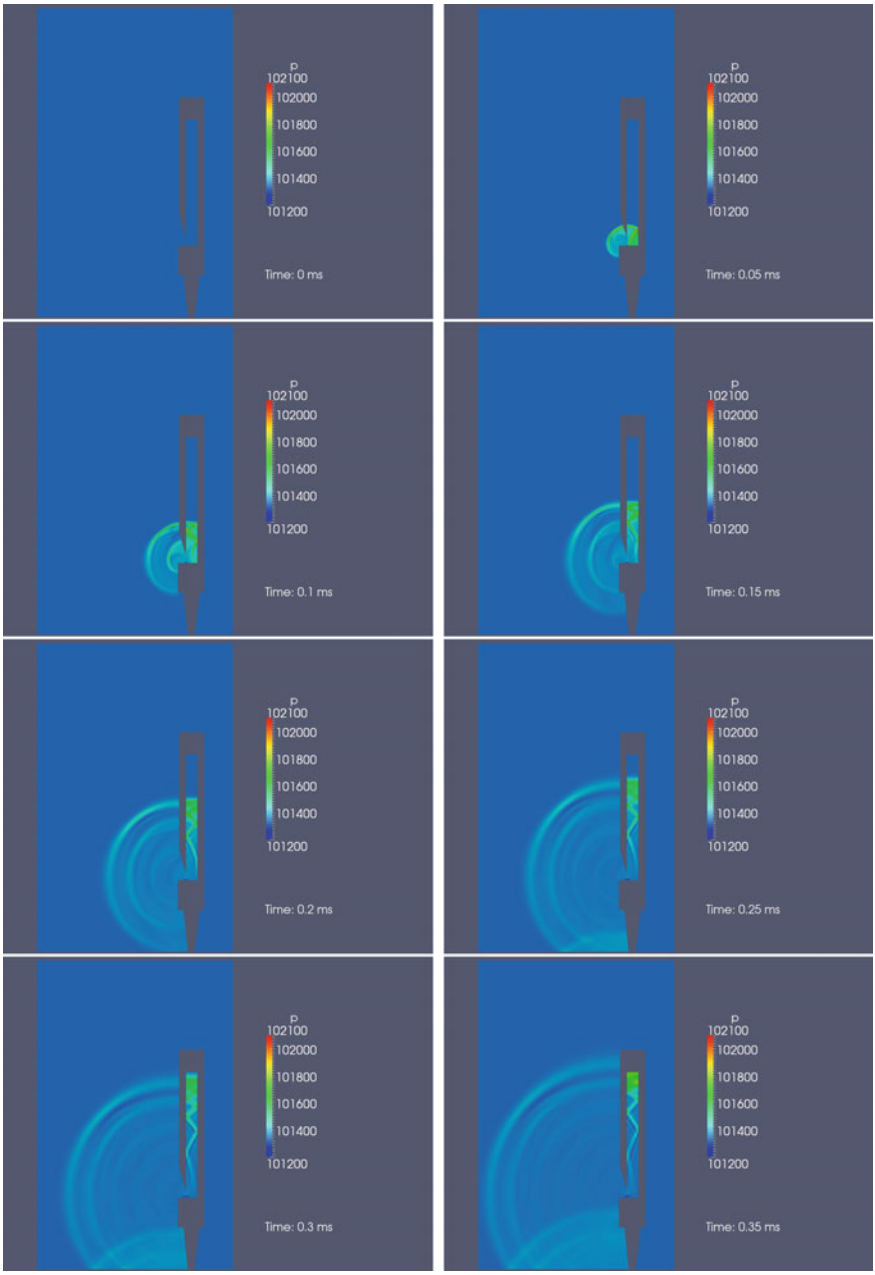


**Fig. 19** Sequence $t = 0-0.35$ ms of the numerical simulation of scenario *swell_125* mm. Shown is the pressure $p$. Depicted is the initial excitation process of the organ pipe and the radiation of a sound wave into the swell chambers space

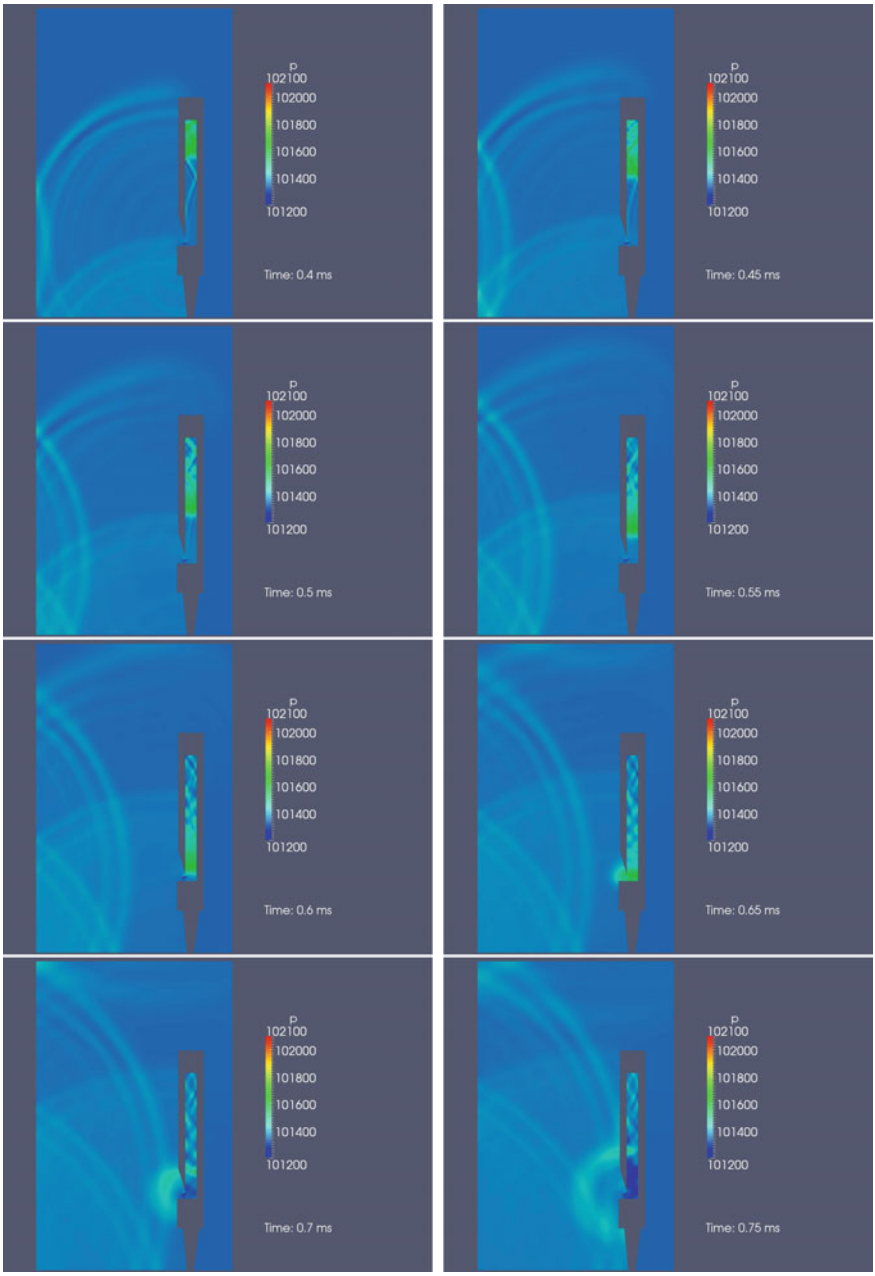


**Fig. 20** Sequence $t = 0.4 - 0.75$ ms of the numerical simulation of scenario *swell_125* mm. Shown is the pressure $p$. Depicted is the initial excitation process of the organ pipe, the radiation of a sound wave into the swell chamber's space, reflection at the swell chamber's walls and back propagation

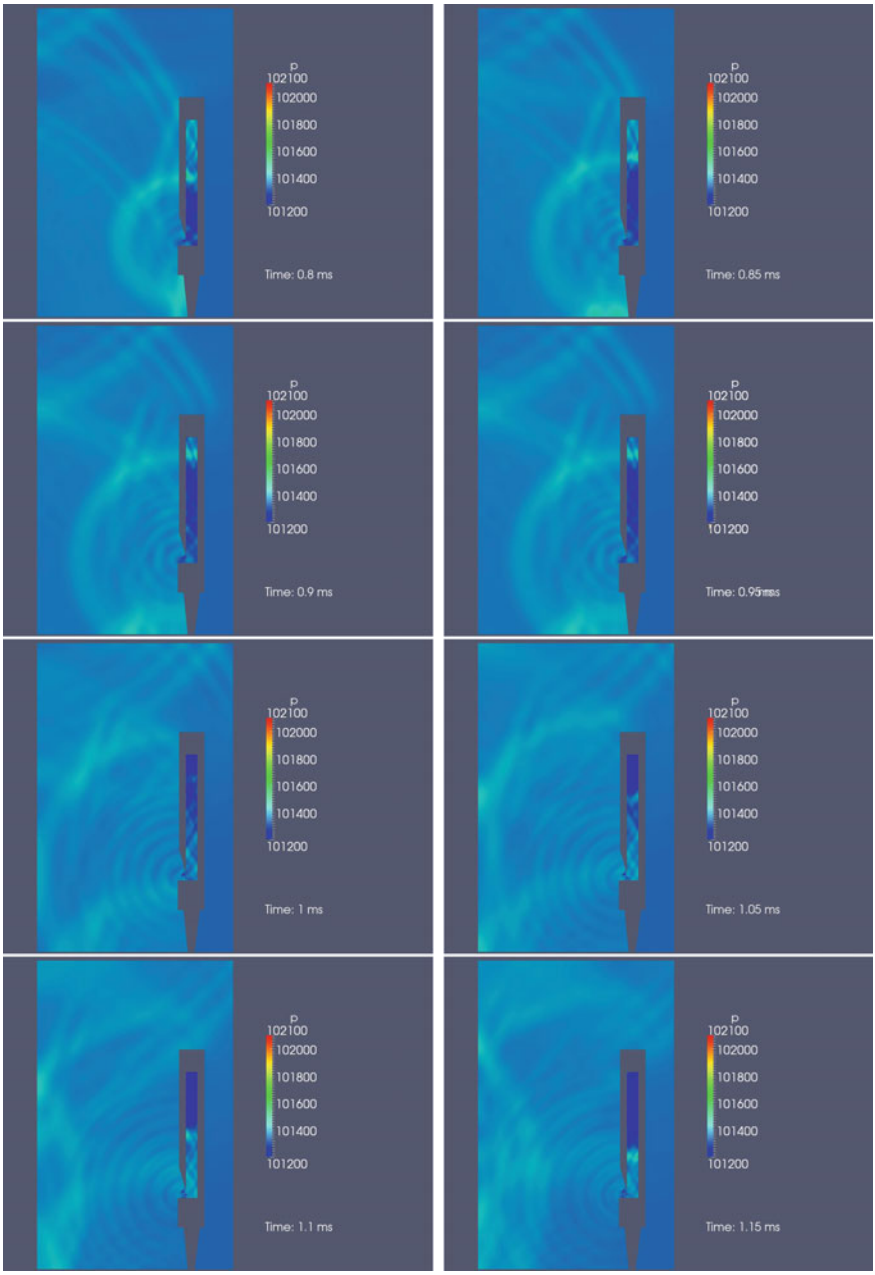


**Fig. 21** Sequence $t = 0.8 - 1.15$ ms of the numerical simulation of scenario *swell_125* mm. Shown is the pressure $p$. Depicted is the initial excitation process of the organ pipe, the radiation of a sound wave into the swell chamber's cavity, reflection at the swell chamber's walls and back propagation

physical values, pressure $p$, velocity magnitude $|U|$, and turbulent kinetic energy $k$, to allow for a detailed qualitative evaluation of the processes within the organ pipe as well as in its surrounding environment.

Figures 19, 20 and 21 show sequences of the computed numerical simulation for the swell chamber configuration *swell_125* mm. Depicted is the initial excitation process. Color-coded is the pressure $p$ in the range of 101200–102100 Pa.

## 4.2 Analysis

For the purpose of analyzing the simulation process, sound pressure level spectra are generated at probe point *C*, i.e., in the upper part of the sealed resonator, as well as at cross-section *cs*0, representing the cut-up. Probe point *C* is selected for its close proximity to the pressure maximum at the upper end of the sealed resonator. The data for cross-section *cs*0 (272 sample points per physical value) are coarse grained by spatial averaging and dividing by the number of sample points.

Thus a SPL-spectrum of the organ pipe's total sound radiation is obtained, reduced to a single point. Both data volumes are of particular interest with regard to an evaluation of the feedback effect of the surrounding room on the sound generation and sound radiation of the organ pipe, for they allow for the investigation of, on the one hand, the effects deep within the organ pipe, in the resonator, and, on the other hand, of the organ pipe's radiation characteristics. Both locations are either very difficult to reach for the purpose of experiment, or not at all. Figure 22 shows

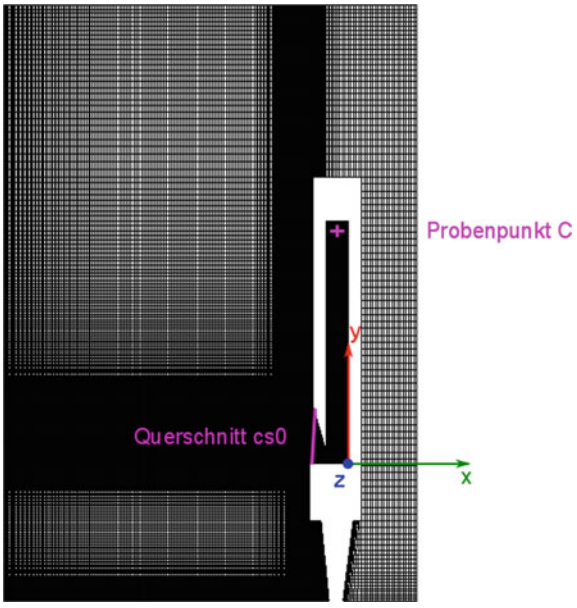


**Fig. 22** Position of the probe point *C* and the cross-section *cs*0 within the mesh

the location of cross-section *cs*0 and the position of probe point *C* (Position [$x = -4.5$ mm, $y = 96$ mm]) within the computational grid.

## 4.3 Sound Pressure Level Spectra Inside the Organ Pipe

Analyzed are the sound pressure level spectra sampled at the probe point *C* for the three numerical simulation runs *free*, *swell_140* mm and *swell_125* mm, shown in Fig. 23a. One observe the fundamental as well as the higher harmonics up to the 13th.

The first harmonics up to the 5th are depicted in Fig. 23b–d.

With simulation *free*, the fundamental oscillation's frequencies as well as the higher harmonics deviate less than 5 % from the values established by experiment.

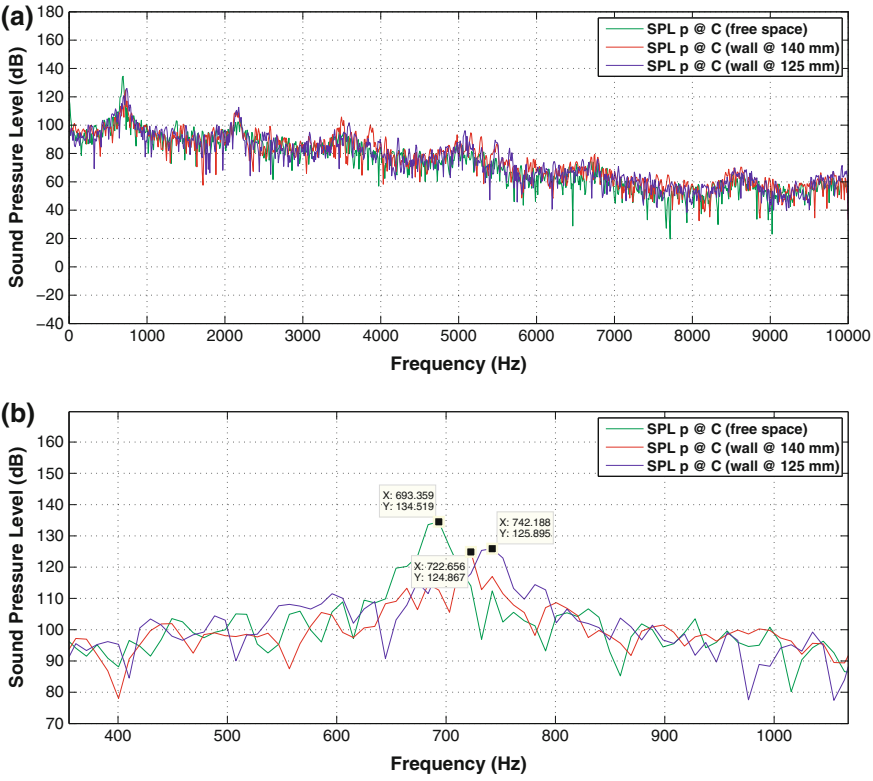


**Fig. 23** SPL-spectra sampled at probe point *C* inside the resonator. **a** SPL-spectra of *free*, *swell_140* mm and *swell_125* mm. **b** Detailed view on the SPL-spectra in the range of the fundamentals. **c** Detailed view on the SPL-spectra in the range of the 3rd harmonics. **d** Detailed view on the SPL-spectra in the range of the 5th harmonics

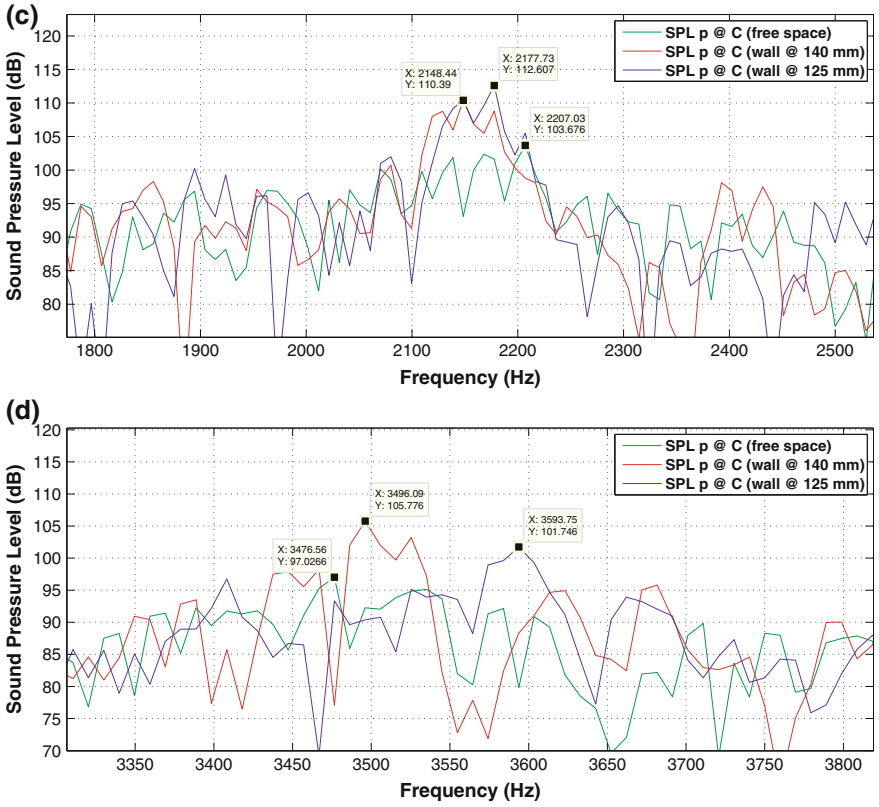


**Fig. 23** (continued)

The simulation thus depicts the behavior of the organ pipe with great precision. The high degree of accuracy remains unaffected when boundary conditions are altered by the introduction of reflective surfaces, as in simulations *swell_140* mm and *swell_125* mm. This is another important quality characteristic of the presented simulations and attests of the robustness and reliability of the techniques applied.

On close examination of the area of fundamental oscillations in Fig. 23b, a frequency shift relative to the reference of approx. $29 \pm 5$ Hz and $49 \pm 5$ Hz, respectively, can be detected in simulation runs *swell_140* mm and *swell_125* mm. Furthermore, the reflecting walls reduce the sound pressure level of the fundamental oscillations by approximately 9.9 and 8.6 dB, respectively. This means that the reflecting walls of the swell chamber significantly affect both frequency and amplitude of the organ pipe. Within a swell chamber that is closed on three sides, the organ pipe undergoes an increase in frequency of the fundamental oscillation as well as a decrease in loudness.

## 4.4 Higher Harmonics

For the perceived sound quality of an organ pipe, the response to higher harmonics is of profound importance. Consequently, 3rd and 5th harmonics will now be evaluated, with simulation run *free* again serving as reference case. The sound pressure level of the 3rd harmonic of *swell_140* mm is 6.7 dB higher than in *free*. The sound pressure level of simulation *swell_125* mm is even higher at 8.9 dB. This means that reflecting surfaces lying in the direction of sound radiation lead to an energy transfer from the fundamental to the 3rd harmonic. This transfer even increases as the distance to the opposing wall is decreased, as is the case with configuration *swell_125* mm. This effect is observable also in the case of the 5th harmonic. The increase is, however, smaller in *swell_125* mm than in *swell_140* mm. In comparison to simulation *free*, the differences amount to 8.7 dB for *swell_140* mm and 4.7 dB for *swell_125* mm. The transfer of energy towards higher harmonics is a highly non-linear process, hitherto not well understood. It is part of current research. To make statements with an even higher degree of precision, the simulated duration would have to be at least doubled, which is, in principle, technically feasible.

## 4.5 Spatially Averaged Sound Pressure Level Spectra of the Cut-up Region

Next is the analysis of the spatially averaged sound pressure level spectra at cross-section *cs*0, spanning the organ pipe's cut-up. By spatially averaging and dividing by the number of sample points (272) the pressure data, the organ pipes total radiation characteristic, reduced into a single point, is obtained.

The sound pressure level spectra thus obtained may be interpreted as the radiation characteristics of the organ pipe, seen as an acoustical point source. The sound pressure level spectra across cross-section *cs*0 are shown in Fig. 24a–c.

In comparison to the sound pressure level spectra of probe point *C*, the frequencies of the fundamental oscillation as well as those of the higher harmonics emerge even more clearly. The increase in frequency of the fundamental, caused by the feedback effect of the swell chamber's reflecting walls, is analogous in behavior to the observations on probe point *C* within the resonator.

The averaged sound pressure levels are slightly lower than within the resonator. This is explained by friction losses at the boundary layer of the inner walls of the resonator affecting the propagating sound wave. At 115.6 dB, the sound pressure level of simulation run *free* corresponds to the experimentally determined values for this organ pipe. The sound pressure levels of the fundamental oscillations in simulation runs *swell_140* mm and *swell_125* mm are, at 103.8 dB and 103.4 dB, respectively, reduced by 11.7 dB and 12.2 dB compared to *free*, equivalent to a decrease by a factor of 4.

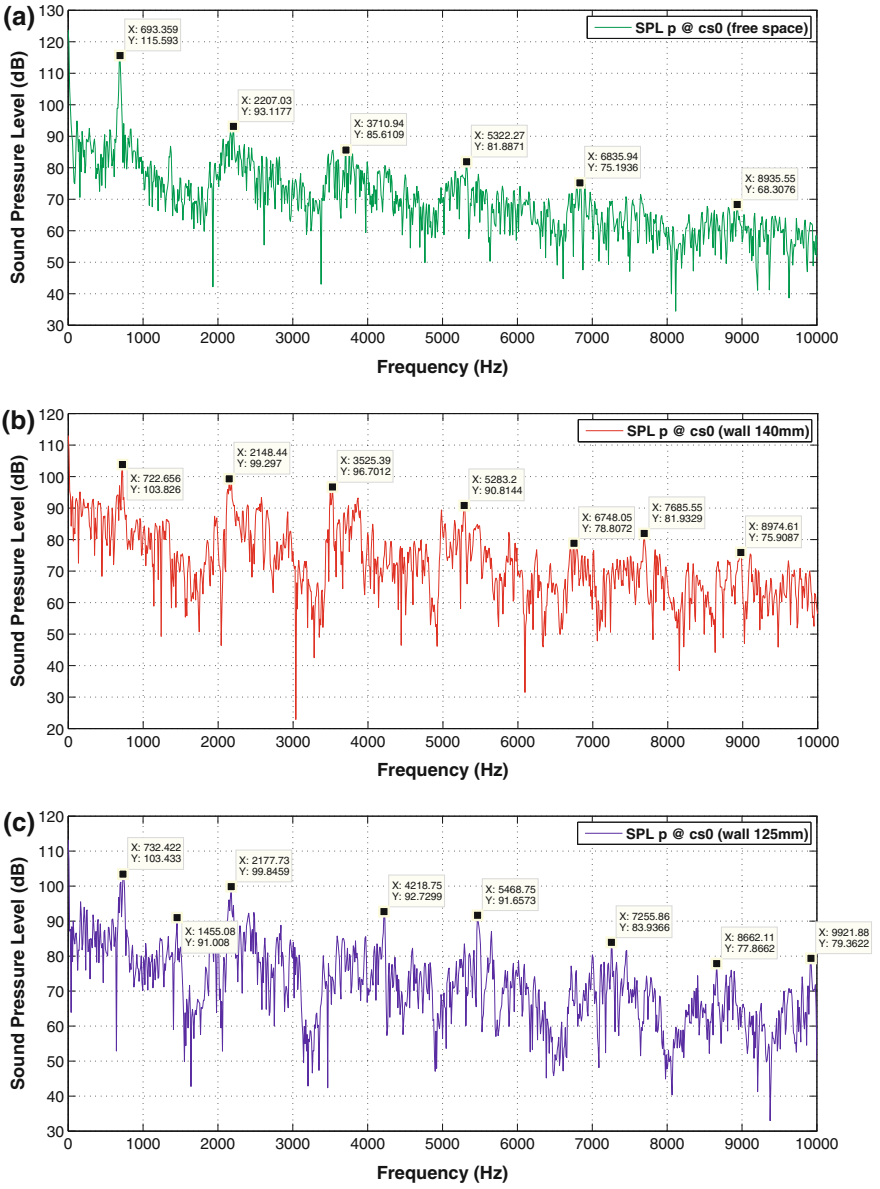


**Fig. 24** Spatially averaged sound pressure level spectra sampled at cross-section *cs*0 of **a** *free*, **b** *swell_140* mm, **c** *swell_125* mm

The energy transfer from the fundamental towards the higher harmonics is more clearly visible as with probe point *C*. It raises the 3rd harmonic by 6.2 dB in *swell_140* mm and by 6.7 dB in *swell_125* mm. In case of the 5th harmonic, an

increase of 11.1 dB and 7.1 dB, respectively, and of 8.9 dB and 9.8 dB, respectively, in case of the 7th harmonic, are observed.

Remarkable, again, is the appearance of a 2nd harmonic in the sound pressure level spectra, as averaged across the cut-up.

In summary it can be stated that the fundamental oscillation is significantly affected by the swell chamber. Depending on the proximity of the organ pipe to an opposing acoustically inert wall, a frequency shift towards higher frequency occurs. Hereby, the fundamental oscillation experiences massive damping, while the higher harmonics are being enhanced. With regard to a more in-depth investigation of these phenomena, further experimentation as well as additional numerical simulations are encouraged.

## 4.6 *Auto-synchronization of the Organ Pipe by Swell Chambers Feedback*

Indications of auto-synchronization of the organ pipe by means of the wall's feedback effects are to be found when analyzing the spatially averaged velocity components across cross-section *cs*0. In Fig. 25a–c, velocity components $v_y$ and $v_x$ are shown, running nearly tangentially and nearly transverse across cross-section *cs*0. It can be seen that, with regard to sound radiation, the fluid dynamical processes and the acoustical processes of sound generation can be well separated. Here, only the acoustical phenomena are discussed. It can clearly be seen that $v_x$ contains mainly the particle velocity, being the velocity component running transverse across cross-section *cs*0.

In the reference scenario, *free*, particle velocity proceeds mostly undisturbed for 80 ms. The simulations incorporating the swell chamber, *swell_140* mm and *swell_125* mm, on the other hand, exhibit interference in the form of period-doubling and beating. These disturbances are caused by sound signals propagating back from the wall with a certain distance-dependent phase shift, interfering with the oscillating jet. Additionally, it has to be taken into account that the particle velocity experiences a sudden phase shift of $\phi_{reflect} = \pi$ at being reflected at the wall, yet sound pressure does not! This is of importance as it is the particle velocity that acts upon the jet.

From theoretical considerations [8, 9] as well as experiments [7, 10], it is known that organ pipes may synchronize under certain circumstances. The interdependencies of sound field and flow field of the jet are discussed in detail in [6].

Mutual cancellation of the particle velocities occurs in the case of both the particle velocity generated on the resonator side, acting upon the jet, and the particle velocity of the reflection, impinging from the outside upon the jet, being offset by $\pi$. As a result, the deflections of the jet come to a standstill, a phenomenon known as oscillation death, or quenching [8].

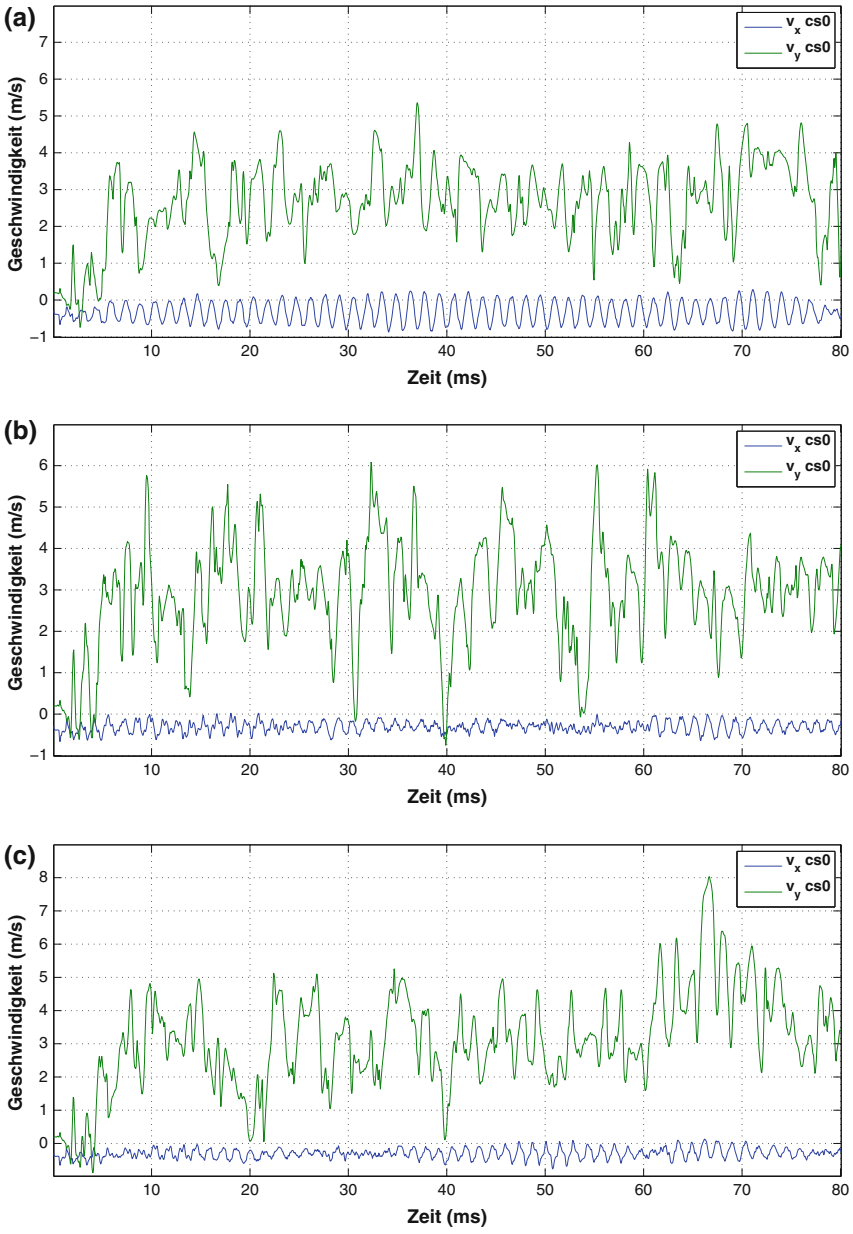


**Fig. 25** Spatially averaged velocity components $v_x$ and $v_y$ at cross-section *cs*0 for **a** the reference scenario*free*, **b** the scenario *swell_140* mm and **c** the scenario *swell_125 mm*. Note that the component $v_x$ is orthogonal to the main time-averaged flow direction of the jet. It can be seen clearly that $v_x$, compared with $v_y$, is much more periodic and with ca. 1/10 lower amplitudes than $v_y$. This indicates that $v_x$ is the carrier of fraction of the sound of the whole signal while the $v_y$ component mainly represents the irregular fraction of the signal, namely the flow of the jet

Based on the results of the analysis, the hypothesis is stated that auto-synchronization, i.e., a synchronization of the jet with its own radiated, reflected, and time delayed sound signal of the same frequency, can occur if the phase difference $\Delta\phi$ of the radiated as well as of the reflected sound signal approaches $\Delta\phi = 0$ and $\Delta\phi = \pi$, respectively. This is equal to the propagation lengths of the sound signal in the surrounding room of multiples of $\lambda$ and $\lambda/2$, respectively. This hypothesis is supported by the decrease in sound pressure level for a distance of propagation of approximately $\lambda/2$ (*swell_125* mm), as discussed above.

## 5 Summary

This chapter dealt with the influence of complex spatial geometries on the sound generation and sound radiation of an organ pipe. The diverging responses of the different wall geometries with regard to the initial sound pressure wave could be clearly distinguished. The processes of sound generation and sound radiation of the organ pipe are significantly affected by the respective spatial geometry of the circumambient room.

Affected are the sound pressure levels of the fundamental oscillation and of the higher harmonics, as well as their frequencies. Particularly noticeable seems to be the variance in the distribution of the sound pressure levels across the fundamental and the higher harmonics. Depending on the spatial geometry, the levels of different frequencies are either accentuated or attenuated, leading to various distinct acoustic patterns for one and the same organ pipe. By selecting a specific spatial geometry, the organ pipe's acoustic pattern may be deliberately altered.

The results of contemplating the effects of swell chambers on sound generation and sound radiation with regard to organ pipes are summarized in note form:

- The acoustic pattern of the organ pipe is significantly affected by the swell chamber.
- The frequency shift caused by the swell chamber's geometry depends on the distance between the organ pipe and the opposite wall.
- Here, a significant distance-dependent decrease in loudness of the fundamental oscillation occurs, as well as an accentuation of higher harmonics.
- The sound pressure level spectra show an energy transfer towards higher harmonics.
- The organ pipe's ability to auto-synchronize with its own radiated sound signal is feasible.

Furthermore, it has been shown that the effects of the circumambient spatial geometry on the organ's sound may be analyzed and displayed by means of numerical simulation in conjunction with the analysis software developed for this purpose, prior to actual organ design and construction. The numerical simulations executed herein allow for further analyses of, e.g., defined cross-sections within the

computational grid as well as of additional physical values that decisively affect the mechanisms of sound generation within the organ pipe and its interdependencies with external parameters.

**Acknowledgments** The author wants to express his gratitude for inspiring discussions with A. Pikovsky, M. Rosenblum, M. Abel and R. Gerhard from University of Potsdam. Many thanks to Alexander Schuke Orgelbau Potsdam GmbH for their active help in pipe and wind supply construction. J. L. Fischer was supported by ZIM, grant "Synchronization in Organ Pipes".

## Bibliography

1. Adelung, W.: Einführung in den Orgelbau. Breitkopf & Hartel, Leipzig (1991)
2. Alexander Schuke Orgelbau Potsdam GmbH. URL http://www.schuke.com/ (2016)
3. OpenFOAM®—The Open Source Computational Fluid Dynamics (CFD) Toolbox Organization—OpenCFD Limited. URL http://www.openfoam.com/ (2016)
4. Morse, P.M., Ingard, K.U.: Theoretical Acoustics. Princeton University Press, Princeton, NJ (1968)
5. Schlichting, H., Gersten, K.: Boundary-layer theory. Springer, Berlin (2003)
6. Fischer, J. L.: Nichtlineare Kopplungsmechanismen akustischer Oszillatoren am Beispiel der Synchronisation von Orgelpfeifen, Ph.D. thesis, available at University of Potsdam (2014)
7. Fischer, J. L.: Über Synchronisationsphänomene nichtlinearer akustischer Oszillatoren, Diploma-thesis, available at University of Potsdam (2012)
8. Pikovsky, A., Rosenblum, M., Kurths, J.: Synchronization—A Universal Concept in Nonlinear Science. Springer, Berlin (2001)
9. Rayleigh, J.W.S.B.: *The* Theory of Sound, Republished 1945 by Dover Publications, New York (1896)
10. Abel, M., Ahnert, K., Bergweiler, B.: Synchronization of sound sources. Phys. Rev. Lett. **1030**, 114301 (2009)

### Author Biography

**Jost Leonhardt Fischer** has been a postdoctoral researcher in the Institute of Systematic Musicology at University of Hamburg, since 2014. His current research focuses on applications of nonlinear dynamics and oscillation theory in musical acoustics. Topics include, inter alia, synchronization phenomena in acoustical waveguides, nonlinearities in sound generation and sound radiation, investigations of the interplay of flows, turbulent layers and sound field as well as numerical simulations of the compressible Navier-Stokes equations. Jost Leonhardt Fischer studied physics at the University of Potsdam, Germany. In his Diploma thesis (2012) he investigated synchronization phenomena of nonlinear acoustic oscillators, from both a numerical and a theoretical perspective. In 2014 he received a Ph.D. in theoretical physics. In his Ph.D. thesis, he studied nonlinear coupling mechanisms of acoustic oscillators with a focus on synchronization of organ pipes.